Double absorbing boundaries for finite-difference time-domain electromagnetics ☆

John LaGrone *, Thomas Hagstrom

Department of Mathematics, Southern Methodist University, PO Box 750156, Dallas, TX 75275, United States

A R T I C L E   I N F O

A B S T R A C T

We describe the implementation of optimal local radiation boundary condition sequences for second order finite difference approximations to Maxwell's equations and the scalar wave equation using the double absorbing boundary formulation. Numerical experiments are presented which demonstrate that the design accuracy of the boundary conditions is achieved and, for comparable effort, exceeds that of a convolution perfectly matched layer with reasonably chosen parameters. An advantage of the proposed approach is that parameters can be chosen using an accurate *a priori* error bound.

© 2016 Elsevier Inc. All rights reserved.

1. Introduction

An important issue in the simulation of electromagnetic effects is the ability to truncate unbounded domains into regions of interest that can be simulated efficiently and accurately for long times. In the context of finite difference time domain (FDTD) solvers, this typically takes the form of a perfectly matched layer (PML) [1]. The PML method is attractive because it is effective and easy to implement; however, the performance is closely tied to a selection of parameters. While work has been done to automate the selection of the optimal PML parameters [2], it is often the case that they must be found by experimentation.

Our goal here is to utilize an alternative to PML, namely the complete radiation boundary conditions (CRBC) [3]. Advantages of the CRBC are:

  i. A clear notion of convergence, exponential in increasing order;
 ii. A sharp *a priori* error estimate;
iii. A fast and inexpensive method for selecting optimized parameters.

Earlier implementations of CRBCs relied on the decomposition of the solution in terms of characteristic variables at the artificial boundary [4]. Due to the staggered grid in time and space used in FDTD methods, it is not readily apparent how to directly implement a CRBC type boundary condition. To deal with these staggered grids, we show how a Double Absorbing Boundary (DAB) [5] can be used to leverage the desirable properties of the CRBCs in FDTD simulations. The DAB

 * Corresponding author.
  E-mail addresses: jlagrone@smu.edu (J. LaGrone), thagstrom@smu.edu (T. Hagstrom).

is constructed by forming a thin non-reflecting layer on which we apply the CRBC on two parallel boundaries. Here we formulate the DAB for the standard second-order central difference approximation to the scalar wave equation satisfied by the components of the electric field, using a 3-point DAB layer. The updated electric field components are then used as boundary data for the staggered grid scheme.

We demonstrate the performance of the method with numerical experiments for problems in waveguides, between parallel plates, and in free space.

2. Double absorbing boundary method

2.1. CRBC review

In order to introduce the DAB method, we first recall that the CRBC [3] is defined recursively using the auxiliary variables $u_0, \ldots, u_P$

$$\bar{a}_j \frac{\partial u_{j+1}}{\partial t} - \frac{\partial u_{j+1}}{\partial \hat{n}} + \bar{\sigma}_j u_{j+1} = a_j \frac{\partial u_j}{\partial t} + \frac{\partial u_j}{\partial \hat{n}} + \sigma_j u_j, \tag{1}$$

where u_0 is the solution in the volume and $\hat{n}$ is the outward pointing normal. The parameters a_j, $\bar{a}_j$, σ_j, and $\bar{\sigma}_j$ are defined as

$$a_j = \frac{\cos \theta_j}{c}, \qquad \bar{a}_j = \frac{\cos \bar{\theta}_j}{c}, \qquad \sigma_j = \frac{1}{cT} \frac{\sin^2 \theta_j}{\cos \theta_j}, \qquad \bar{\sigma}_j = \frac{1}{cT} \frac{\sin^2 \bar{\theta}_j}{\cos \bar{\theta}_j}, \tag{2}$$

where the angle variables θ_j and $\bar{\theta}_j$ are chosen to minimize the reflections, c is the wave speed, and T is the total time of interest (e.g. the simulation time). Here we assume u_0 satisfies the scalar wave equation in the vicinity of the artificial boundary and beyond:

$$\frac{\partial^2 u_0}{\partial t^2} - c^2 \nabla^2 u_0 = 0. \tag{3}$$

After defining a separation parameter δ to be the minimum separation between the boundary and any scatterers, sources, or other inhomogeneities, in [3] it is shown that the maximum reflection coefficient is given by

$$\rho = \max_{0 \le \theta < \pi/2} \left(\prod_{j=0}^{P-1} \frac{|\cos\theta - a_j||\cos\theta - \bar{a}_j|}{(\cos\theta + a_j)(\cos\theta + \bar{a}_j)} \right) \cdot \left(\frac{1 - \cos\theta}{1 + \cos\theta} \right) e^{-\frac{\delta}{cT} \frac{1}{\cos\theta}}. \tag{4}$$

An optimization scheme can be employed to rapidly select the parameters a_j and $\bar{a}_j$ that minimize ρ. It can be proven that ρ decreases exponentially with P. Precisely,

$$P \propto \ln\left(\frac{1}{\rho}\right) \cdot \ln\left(\frac{cT}{\delta}\right). \tag{5}$$

Functions which compute these parameters are included in our CRBC software library **rbcpack** (www.rbcpack.org). We emphasize that the angle variables are *not incidence angles of plane waves*. Rather they parameterize a complete wave representation as derived in [3]. As such the reflection coefficient ρ provides an *a priori* error estimate. More precisely, since ρ is an upper bound for the reflection error along an entire inversion contour for a Fourier–Laplace representation of the solution in the far field, a direct application of Parseval's relation implies a simple error bound which is attained for some data. Moreover, as the optimization is based on the equidistribution principle, one expects it to be rather accurate for broadband signals. We will see in the numerical experiments that the predicted accuracy can be attained for sufficiently well-resolved waves and that the error bounds are sharp.

2.2. DAB for the scalar wave equation

Following from [5], to illustrate the DAB method, we consider the scalar wave equation in the semi-bounded domain as shown in Fig. 1(a)

$$\frac{\partial^2 u}{\partial t^2} - c^2 \nabla^2 u = f. \tag{6}$$

For simplicity, we prescribe zero Dirichlet conditions on the boundaries

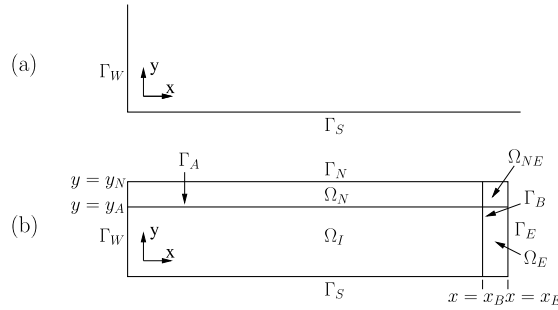$$u = 0, \quad \text{on } \Gamma_W, \Gamma_S, \tag{7}$$

and initial conditions

Fig. 1. (a) The original domain, (b) the truncated domain.

$$u(x, y, t = 0) = h(x, y), \tag{8}$$

$$\frac{\partial u}{\partial t}(x, y, t = 0) = g(x, y), \tag{9}$$

where h and g are known functions satisfying the boundary conditions. We further require that c is constant, $f = 0$, and the initial values vanish outside a compact region, Ω_0.

We next truncate the semi-infinite domain by introducing two artificial boundaries: Γ_N and Γ_E located at $y = y_N$ and $x = x_E$, respectively. We additionally introduce two interfaces Γ_A and Γ_B which are located at $y = y_A < y_N$ and $x = x_B < x_E$, respectively. The entire computation domain, Ω, is bounded by $\Gamma_N \bigcup \Gamma_E \bigcup \Gamma_S \bigcup \Gamma_W$. As shown in Fig. 1(b), this divides the computational domain into four subdomains: the interior domain Ω_I; two thin edge layers, Ω_N and Ω_E; and a thin corner layer Ω_{NE}. We suppose the interfaces Γ_A and Γ_B are chosen such that $\Omega_0 \subset \Omega_I$; therefore, in the layers Ω_N, Ω_E, and Ω_{NE}, c is constant, $f = 0$, and the initial conditions are zero.

The idea is to use the thin layers Ω_N, Ω_E, and Ω_{NE} as absorbing layers so that we may compute the solution in Ω_I as close to the solution of the semi-infinite problem as possible. To do this, we introduce a set of auxiliary variables in each of the layers. In Ω_N, we introduce $\phi_0, ..., \phi_Q$; in Ω_E we introduce $\upsilon_0, ..., \upsilon_P$; and in Ω_{NE} we introduce the doubly indexed set of auxiliary variables $\psi_{p,q}$ with $p = 0, ..., P$ and $q = 0, ..., Q$. In each layer, we require the auxiliary variables to satisfy (6) with $f = 0$:

$$\frac{\partial^2 \phi_q}{\partial t^2} - c^2 \nabla^2 \phi_q = 0, \quad \text{in } \Omega_N, \tag{10}$$

$$\frac{\partial^2 \upsilon_p}{\partial t^2} - c^2 \nabla^2 \upsilon_p = 0, \quad \text{in } \Omega_E, \tag{11}$$

$$\frac{\partial^2 \psi_{p,q}}{\partial t^2} - c^2 \nabla^2 \psi_{p,q} = 0, \quad \text{in } \Omega_{NE}. \tag{12}$$

We insist that the auxiliary variables satisfy zero initial conditions and we apply the same boundary conditions as u on Γ_S and Γ_W:

$$\phi_q = 0, \qquad \text{on } \Gamma_W, \tag{13}$$

$$\upsilon_p = 0, \qquad \text{on } \Gamma_S. \tag{14}$$

In order to couple the auxiliary variables in the layers and the interior, we require that the CRBC recursions (1) be satisfied on the boundaries:

$$\left(\bar{a}_q \frac{\partial}{\partial t} - \frac{\partial}{\partial y} + \bar{\sigma}_q \right) \phi_{q+1} = \left(a_q \frac{\partial}{\partial t} + \frac{\partial}{\partial y} + \sigma_q \right) \phi_q, \quad \text{on } \Gamma_A, \ \Gamma_N, \tag{15}$$

$$\left(\bar{b}_p \frac{\partial}{\partial t} - \frac{\partial}{\partial x} + \bar{\varsigma}_p \right) \upsilon_{p+1} = \left(b_p \frac{\partial}{\partial t} + \frac{\partial}{\partial x} + \varsigma_p \right) \upsilon_p, \quad \text{on } \Gamma_B, \ \Gamma_E, \tag{16}$$

and for the auxiliary variables defined on the corner layer, Γ_{NE}, we require

$$\left(\bar{a}_q \frac{\partial}{\partial t} - \frac{\partial}{\partial y} + \bar{\sigma}_q \right) \psi_{p,q+1} = \left(a_q \frac{\partial}{\partial t} + \frac{\partial}{\partial y} + \sigma_q \right) \psi_{p,q}, \quad \text{on } \Gamma_A, \ \Gamma_N, \tag{17}$$

$$\left(\bar{b}_p \frac{\partial}{\partial t} - \frac{\partial}{\partial x} + \bar{\varsigma}_p \right) \psi_{p+1,q} = \left(b_p \frac{\partial}{\partial t} + \frac{\partial}{\partial x} + \varsigma_p \right) \psi_{p,q}, \quad \text{on } \Gamma_B, \ \Gamma_E. \tag{18}$$

To begin the recursions on the interior sides of the layer, we require the slope and value of ϕ_0 and υ_0 to coincide with u:

$$\phi_0 = u, \quad \frac{\partial \phi_0}{\partial y} = \frac{\partial u}{\partial y}, \quad \text{on } \Gamma_A, \tag{19}$$

$$\upsilon_0 = u, \quad \frac{\partial \upsilon_0}{\partial x} = \frac{\partial u}{\partial x}, \quad \text{on } \Gamma_B. \tag{20}$$

In the corner layer, we require the zeroth level of the auxiliary variable in each direction to agree in slope and value with the auxiliary variables in the neighboring layer,

$$\psi_{p,0} = \phi_p, \quad \frac{\partial \psi_{p,0}}{\partial x} = \frac{\partial \phi_p}{\partial x}, \quad p = 0, ..., P, \quad \text{on } \Gamma_B, \tag{21}$$

$$\psi_{0,q} = \upsilon_q, \quad \frac{\partial \psi_{0,q}}{\partial y} = \frac{\partial \upsilon_q}{\partial y}, \quad q = 0, ..., Q, \quad \text{on } \Gamma_A. \tag{22}$$

On the exterior sides of the layers, we terminate the recursions using the Sommerfeld conditions

$$\left(\frac{\partial}{\partial t} + c \frac{\partial}{\partial y} \right) \phi_Q = 0, \quad \text{on } \Gamma_N, \tag{23}$$

$$\left(\frac{\partial}{\partial t} + c \frac{\partial}{\partial x} \right) \upsilon_P = 0, \quad \text{on } \Gamma_E, \tag{24}$$

$$\left(\frac{\partial}{\partial t} + c \frac{\partial}{\partial y} \right) \psi_{p,Q} = 0, \quad p = 0, ..., P, \quad \text{on } \Gamma_N, \tag{25}$$

$$\left(\frac{\partial}{\partial t} + c \frac{\partial}{\partial x} \right) \psi_{P,q} = 0, \quad q = 0, ..., Q, \quad \text{on } \Gamma_E. \tag{26}$$

Since the auxiliary variables are continuous across the interfaces at the zeroth level by construction and satisfy the same wave equation as u, we have

$$\phi_0 \equiv u, \quad \text{in } \Omega_N, \tag{27}$$

$$\upsilon_0 \equiv u, \quad \text{in } \Omega_E, \tag{28}$$

$$\psi_{0,0} \equiv u, \quad \text{in } \Omega_{NE}. \tag{29}$$

We note that the extension to a full three dimensional problem is analogous and simply requires the introduction of a set of triply indexed auxiliary variables to handle corners.

2.3. Discretization

To discretize the DAB, we use finite differences in space and time. We define the grid spacings in x and y to be h_x and h_y, respectively, and discretize time with the time-step size Δt. In order to more efficiently write the finite difference scheme, we introduce the following discrete operators:

$$\begin{aligned}
\text{Forward average in space:} \quad & A_x^+ v_{i,j} = (v_{i,j} + v_{i+1,j})/2, \\
\text{Forward average in time:} \quad & A_t^+ v^n = (v^n + v^{n+1})/2, \\
\text{Forward difference in space:} \quad & D_x^+ v_{i,j} = (v_{i+1,j} - v_{i,j})/h_x, \\
\text{Backward difference in space:} \quad & D_x^- v_{i,j} = (v_{i,j} - v_{i-1,j})/h_x, \\
\text{Forward difference in time:} \quad & D_t^+ v^n = (v^{n+1} - v^n)/\Delta t, \\
\text{Backward difference in time:} \quad & D_t^- v^n = (v^n - v^{n-1})/\Delta t,
\end{aligned} \tag{30}$$

and analogously define A_y^+, D_y^+, and D_y^-. Then we can discretize the interior of the problem (6), Γ_I, using standard second order central differences

$$D_t^+ D_t^- u_{i,j}^n = c^2 \left(D_x^+ D_x^- + D_y^+ D_y^- \right) u_{i,j}^n + f_{i,j}^n,$$
$$i = 1, ..., n_x - 1, \quad j = 1, ..., n_y - 1, \quad n \geq 1, \tag{31}$$

where there are $(n_x + 1)$ and $(n_y + 1)$ grid points in the x and y directions, respectively, and $u_{i,j}^n \approx u(x_i, y_j, n\Delta t)$, $f_{i,j}^n = f(x_i, y_j, n\Delta t)$, and Δt has been chosen to satisfy the CFL condition

$$\Delta t \leq c^{-1} \left((h_x)^{-2} + (h_y)^{-2} \right)^{-1/2}. \tag{32}$$

We note that setting $u_{i,j}^n = 0$ satisfies the boundary conditions whenever $i = 0$ or $j = 0$, so these values do not require updates.

To discretize the layers Ω_E, Ω_N, and Ω_{NE}, we note that they only need to be wide enough to support the wave equation stencil. In the case of second order centered differences, this means that we only require the layers to be three grid points (or $2h$) wide. The layers can be made thicker, but there is no practical benefit [5]. Therefore, Ω_N has $(n_x + 1)$ gridpoints in the x direction and 3 gridpoints in the y direction; Ω_E has 3 gridpoints in the x direction and $(n_y + 1)$ gridpoints in the y direction; and Ω_{NE} has 3 gridpoints in each direction. For clarity we index these points in accordance with the interior indexing; for example in Ω_N the auxiliary functions have a second index ranging from $n_y - 1$ to $n_y + 1$. Then the updates for the interiors of the layers are given by discretizing (10)–(12):

$$D_t^+ D_t^- \phi_{i,n_y,q}^n = c^2 \left(D_x^+ D_x^- + D_y^+ D_y^- \right) \phi_{i,n_y,q}^n,$$
$$i = 1, \ldots, n_x - 1, \quad q = 0, \ldots, Q, \tag{33}$$

$$D_t^+ D_t^- \upsilon_{n_x,j,p}^n = c^2 \left(D_x^+ D_x^- + D_y^+ D_y^- \right) \upsilon_{n_x,j,p}^n,$$
$$j = 1, \ldots, n_y - 1, \quad p = 0, \ldots, P, \tag{34}$$

$$D_t^+ D_t^- \psi_{n_x,n_y,p,q}^n = c^2 \left(D_x^+ D_x^- + D_y^+ D_y^- \right) \psi_{n_x,n_y,p,q}^n,$$
$$q = 0, \ldots, Q, \quad p = 0, \ldots, P. \tag{35}$$

The CRBC recursions on the interface side of the layers given in (15)–(16) are discretized as

$$\left(\bar{a}_q D_t^+ A_y^+ - D_y^+ A_t^+ + \bar{\sigma}_q A_t^+ A_y^+ \right) \phi_{i,j,q+1}^n =$$
$$\left(a_q D_t^+ A_y^+ + D_y^+ A_t^+ + \sigma_q A_t^+ A_y^+ \right) \phi_{i,j,q}^n,$$
$$i = 1, \ldots, n_x - 1, \quad j = n_y - 1, n_y, \tag{36}$$

$$\left(\bar{b}_p D_t^+ A_x^+ - D_x^+ A_t^+ + \bar{\varsigma}_p A_t^+ A_x^+ \right) \upsilon_{i,j,p+1}^n =$$
$$\left(b_p D_t^+ A_x^+ + D_x^+ A_t^+ + \varsigma_p A_t^+ A_x^+ \right) \upsilon_{i,j,p}^n,$$
$$i = n_x - 1, n_x, \quad j = 1, \ldots, n_y - 1. \tag{37}$$

The recursions on the sides of the corner layer Ω_{NE} given in (17)–(18) are discretized analogously as

$$\left(\bar{a}_q D_t^+ A_y^+ - D_y^+ A_t^+ + \bar{\sigma}_q A_t^+ A_y^+ \right) \psi_{n_x,j,p,q+1}^n =$$
$$\left(a_q D_t^+ A_y^+ + D_y^+ A_t^+ + \sigma_q A_t^+ A_y^+ \right) \psi_{n_x,j,p,q}^n, \quad j = n_y - 1, n_y, \tag{38}$$

$$\left(\bar{b}_p D_t^+ A_x^+ - D_x^+ A_t^+ + \bar{\varsigma}_p A_t^+ A_x^+ \right) \psi_{i,n_y,p+1,q}^n =$$
$$\left(b_p D_t^+ A_x^+ + D_x^+ A_t^+ + \varsigma_p A_t^+ A_x^+ \right) \psi_{i,n_y,p,q}^n, \quad i = n_x - 1, n_x,. \tag{39}$$

We can solve the "forward" recursions on Γ_A and Γ_B from (36)–(39) and for $\phi_{i,n_y-1,q+1}^{n+1}$, $\upsilon_{n_x-1,j,p+1}^{n+1}$, $\psi_{n_x,n_y-1,p,q+1}^{n+1}$, and $\psi_{n_x-1,n_y,p+1,q}^{n+1}$. Similarly, we can solve the "backward" recursions on Γ_N and Γ_E for $\phi_{i,n_y+1,q}^{n+1}$, $\upsilon_{n_x+1,j,p}^{n+1}$, $\psi_{n_x,n_y+1,p,q}^{n+1}$, and $\psi_{n_x+1,n_y,p,q}^{n+1}$. We note this yields explicit update formulas, which we enumerate in Appendix A.

Finally, the termination conditions (23)–(26) are discretized as

$$(D_t^+ A_y^+ + c D_y^+ A_t^+) \phi_{i,n_y+1,Q}^n = 0, \quad i = 1, \ldots, n_x - 1, \tag{40}$$

$$(D_t^+ A_x^+ + c D_x^+ A_t^+) \upsilon_{n_x+1,j,P}^n = 0, \quad j = 1, \ldots, n_y - 1, \tag{41}$$

$$(D_t^+ A_y^+ + c D_y^+ A_t^+) \psi_{n_x,n_y+1,p,Q}^n = 0, \quad p = 0, \ldots P, \tag{42}$$

$$(D_t^+ A_x^+ + c D_x^+ A_t^+) \psi_{n_x+1,n_y,P,q}^n = 0, \quad q = 0, \ldots Q. \tag{43}$$

Again, we can solve the equations (40)–(43) to yield explicit updates for $\phi_{i,n_y+1,Q}^{n+1}$, $\upsilon_{n_x+1,j,P}^{n+1}$, $\psi_{n_x,n_y+1,p,Q}^{n+1}$, and $\psi_{n_x+1,n_y,P,q}^{n+1}$.

Then the full update procedure is:

1. Update the internal grid points using (31).
2. Copy the new internal values to zeroth level of the auxiliary variables. Specifically, copy v_{i,n_y-1}^{n+1} to $\phi_{i,n_y-1,0}^{n+1}$ and copy $u_{n_x-1,j}^{n+1}$ to $\upsilon_{n_x-1,j,0}^{n+1}$.
3. Update the internal points of Ω_N and Ω_E using (33)–(34).
4. Apply the termination conditions (40)–(41) to the points in Ω_N and Ω_E.
5. Update the points in Ω_N and Ω_E using the recursions (36)–(37).

6. Copy the updated auxiliary variables from Ω_N and Ω_E to the zeroth level auxiliary variables in Ω_{NE}. Specifically, copy $\phi^{n+1}_{n_x-1,n_y,q}$ to $\psi^{n+1}_{n_x-1,n_y,0,q}$ and $\upsilon^{n+1}_{n_x,n_y-1,p}$ to $\psi^{n+1}_{n_x,n_y-1,p,0}$.
7. Compute the updates to $\psi^{n+1}_{n_x,n_y,p,q}$ using (35).
8. Apply the termination conditions (42)–(43) to the points in Ω_{NE}.
9. Apply the recursive updates (38)–(39).
10. Copy the updated values from Ω_{NE} into Ω_N and Ω_E. In particular, copy $\psi^{n+1}_{n_x,n_y,0,q}$ to $\phi^{n+1}_{n_x,n_y,q}$ and $\psi^{n+1}_{n_x,n_y,p,0}$ to $\upsilon^{n+1}_{n_x,n_y,p}$.
11. Copy the updated values from Ω_N and Ω_E into Ω_I. In particular, copy $\phi^{n+1}_{i,n_y,0}$ to u^{n+1}_{i,n_y} and $\upsilon^{n+1}_{n_x,j,0}$ to $u^{n+1}_{n_x,j}$.
12. Move to the next time step $n \leftarrow n+1$.

Notice that we only require updates to the points in the wave equation's stencil. In particular, we do not need to update the points in the corners of Ω_{NE}. Finally, note that we can handle other boundary condition types by modifying the wave equation updates (33)–(34). For example, if on Γ_W we instead imposed a zero Neumann condition, we would modify the wave equation updates at Γ_W in Ω_N to be

$$D_t^+ D_t^- \phi^n_{0,n_y,q} = c^2 \left(\frac{\phi^n_{1,n_y,q} - \phi^n_{0,n_y,q}}{h^2} + D_y^+ D_y^- \phi^n_{0,n_y,q} \right), \quad q = 0, ..., Q, \tag{44}$$

which we arrive at by substituting $D_x^- \phi^n_{0,n_y,q} = 0$.

3. Application to the Yee scheme

In order to apply the DAB to the Yee scheme, we require the material in the neighborhood of the boundaries to be homogeneous, isotropic, and dielectric. In this case, Maxwell's equations are given by

$$\frac{\partial \mathbf{H}}{\partial t} = -\frac{1}{\mu} \nabla \times \mathbf{E}, \tag{45}$$

$$\frac{\partial \mathbf{E}}{\partial t} = \frac{1}{\varepsilon} \nabla \times \mathbf{H}, \tag{46}$$

subject to the constraints

$$\nabla \cdot \mathbf{E} = 0, \tag{47}$$

$$\nabla \cdot \mathbf{H} = 0. \tag{48}$$

We emphasize that there can be any number of sources, scatterers, or other inhomogeneities in the interior of the domain so long as they are separated from the DAB boundaries by some distance $\delta > 0$.

To discretize these equations using Yee's scheme [6] on a rectangular domain $[x_L, x_R] \times [y_L, y_R] \times [z_L, z_R]$ with mesh spacings of h_x, h_y, and h_z, in the x, y, and z directions, respectively, we define

$$x_i = x_L + i h_x, \qquad y_j = y_L + j h_y, \qquad z_k = z_L + k h_z. \tag{49}$$

We choose a time step size, Δt, satisfying

$$\Delta t \leq c^{-1} \left((h_x)^{-2} + (h_y)^{-2} + (h_z)^{-2} \right)^{-1/2}, \tag{50}$$

with the wave speed, $c = (\varepsilon \mu)^{-1/2}$. Letting

$$t_n = n\Delta t, \tag{51}$$

Maxwell's equations are approximated on a staggered space–time grid:

$$D_t^+ (H_x)^n_{i,j+1/2,k+1/2} = \frac{1}{\mu} \left(D_z^+ (E_y)^{n+1/2}_{i,j+1/2,k} - D_y^+ (E_z)^{n+1/2}_{i,j,k+1/2} \right), \tag{52}$$

$$D_t^+ (H_y)^n_{i+1/2,j,k+1/2} = \frac{1}{\mu} \left(D_x^+ (E_z)^{n+1/2}_{i,j,k+1/2} - D_z^+ (E_x)^{n+1/2}_{i+1/2,j,k} \right), \tag{53}$$

$$D_t^+ (H_z)^n_{i+1/2,j+1/2,k} = \frac{1}{\mu} \left(D_y^+ (E_x)^{n+1/2}_{i+1/2,j,k} - D_x^+ (E_y)^{n+1/2}_{i,j+1/2,k} \right), \tag{54}$$

$$D_t^- (E_x)^{n+1/2}_{i+1/2,j,k} = \frac{1}{\varepsilon} \left(D_y^- (H_z)^n_{i+1/2,j+1/2,k} - D_z^- (H_y)^n_{i+1/2,j,k+1/2} \right), \tag{55}$$

$$D_t^- (E_y)^{n+1/2}_{i,j+1/2,k} = \frac{1}{\varepsilon} \left(D_z^- (H_x)^n_{i,j+1/2,k+1/2} - D_x^- (H_z)^n_{i+1/2,j+1/2,k} \right), \tag{56}$$

$$D_t^- (E_z)^{n+1/2}_{i,j,k+1/2} = \frac{1}{\varepsilon} \left(D_x^- (H_y)^n_{i+1/2,j,k+1/2} - D_y^- (H_x)^n_{i,j+1/2,k+1/2} \right). \tag{57}$$

Table 1
Simulation results for the Transverse Magnetic problem in Free Space.

Grid	DoFs	BC	Max Rel Err
3000×3000	2.72×10^7	DAB $P = 5$	3.73×10^{-4}
3000×3000	2.73×10^7	DAB $P = 9$	2.76×10^{-5}
10000×10000	3.01×10^8	DAB $P = 9$	2.72×10^{-6}
3000×3000	2.76×10^7	PML	2.76×10^{-5}
10000×10000	3.02×10^8	PML	1.69×10^{-5}

Note that if the initial data is discretely divergence free, it is easy to verify that discretizations of (47) and (48) are automatically enforced by the update scheme. Furthermore, it can be shown that each of the field components satisfies the standard second order central difference approximation to the scalar wave equation, e.g.

$$D_t^+ D_t^- (E_x)_{i+1/2,j,k}^{n+1/2} = c^2 \left(D_x^+ D_x^- + D_y^+ D_y^- + D_z^+ D_z^- \right) (E_x)_{i+1/2,j,k}^{n+1/2}. \tag{58}$$

Therefore, we can use the DAB formulation given in Sec. 2.2 for each **E** field component. We want to emphasize that CRBC-type boundary conditions can be directly applied to Maxwell's equations in other discretizations, but it is not readily apparent that this is possible to do in the Yee scheme because of the staggered space–time grid. For instance, CRBCs are successfully applied to a discontinuous Galerkin method in [7] by applying the CRBC recursions (1) to the characteristic equations for Maxwell's equations.

In principle, we should only be required to update the tangential **E** field values on the DAB boundaries to provide the correct number of boundary conditions. However, in the cases where there are DAB layers meeting at edges or corners, we require information from the normal **E** field auxiliary components. It is our belief that it should be possible to obtain this information without applying the DAB conditions to the normal **E** field component on the boundary (e.g. using the divergence free condition (47)), but our current implementation involves the evolution of all three components on adjacent DAB layers. Full details are given in Appendix B.

4. Numerical results

4.1. Free space transverse magnetic

We simulated the free space transverse magnetic problem given by

$$\mu \frac{\partial H_x}{\partial t} = -\frac{\partial E_z}{\partial y},$$
$$\mu \frac{\partial H_y}{\partial t} = \frac{\partial E_z}{\partial x}, \tag{59}$$
$$\varepsilon \frac{\partial E_z}{\partial t} = \frac{\partial H_y}{\partial x} - \frac{\partial H_x}{\partial y}.$$

To start the simulation, we take initial data from a solution of the form

$$E_z = \mu \frac{\partial w}{\partial t}, \qquad H_x = -\frac{\partial w}{\partial y}, \qquad H_y = \frac{\partial w}{\partial x}, \tag{60}$$

where w is a solution of the scalar wave equation produced by a point source centered at $(0, 0.1)$ with the time amplitude $\exp\left(-125(t + .475)^2\right)$. The DAB boundaries were placed at $x = \pm 1$ and $y = \pm 1$. The errors reported are relative to the initial condition and are given by the following formula

$$e_{rel}^n = \sqrt{\frac{\varepsilon \left\| \mathbf{E}_{\text{approx}}^{n+1/2} - \mathbf{E}_{\text{exact}}^{n+1/2} \right\|_2^2 + \mu \left\| \mathbf{H}_{\text{approx}}^n - \mathbf{H}_{\text{exact}}^n \right\|_2^2}{\varepsilon \left\| \mathbf{E}_{\text{exact}}^{1/2} \right\|_2^2 + \mu \left\| \mathbf{H}_{\text{exact}}^0 \right\|_2^2}} \tag{61}$$

Here we compare our results to those obtained using 10-point convolution PML (PML) [8] with parameters $\alpha_{max} = 0.25$, $\kappa_{max} = 0.15$, and $\sigma_{max} \approx 5000$ for the coarse grid and $\sigma_{max} \approx 16700$ for the refined grid. These parameters were selected based on the recommendations from [8]. The proposed formulation with $P = 9$ uses fewer degrees-of-freedom than the PML but achieves the same short-time accuracy and better long-time accuracy with the same interior grid of 3000^2 E_z grid points; see Fig. 2, Table 1. With further refinement the error is reduced by an order of magnitude and achieves the *a priori* error estimate. Before the wave reaches the boundary, we see only discretization error. After impact, the boundary error dominates the simulation. This is particularly evident when comparing the simulations with $P = 5$ and $P = 9$ on the same grid as the difference in error is entirely due to the boundary condition order. We believe that the error in the PML
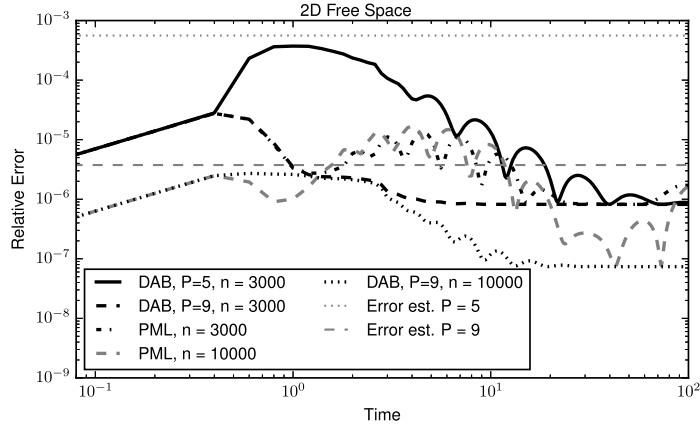
Fig. 2. Relative Error in Free Space for the Transverse Magnetic Test Problem.
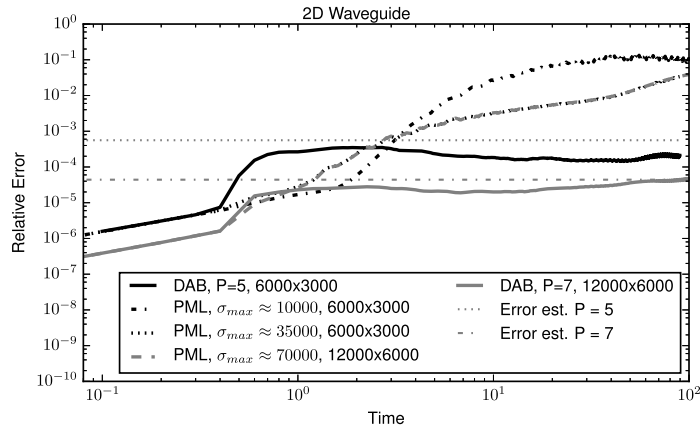

Fig. 3. Relative Error for the Transverse Magnetic Test Problem in a Waveguide computed according to (61). Maximum relative errors can be seen in Table 2.

Table 2
Simulation results for the Transverse Magnetic problem in a Waveguide.

Grid	DoFs	BC	Max Rel Err
6000×3000	5.41×10^7	DAB $P = 5$	3.52×10^{-4}
12000×6000	2.16×10^8	DAB $P = 7$	4.82×10^{-5}
6000×3000	5.43×10^7	PML, $\sigma_{max} \approx 35000$	3.37×10^{-2}
6000×3000	5.43×10^7	PML, $\sigma_{max} \approx 10000$	1.33×10^{-1}
12000×6000	2.17×10^8	PML, $\sigma_{max} \approx 70000$	3.88×10^{-2}

boundary increases after a short time because the wave impacts the exterior boundary of the PML and reflects back into the interior domain, but we note that the overall performance is similar to $P = 9$ and may be improved with better PML parameter selection. Finally, the fact that the error decreases in stages for the boundaries is an indication that a wave is reflected and then at least partially absorbed once it travels to the other side of the domain.

### 4.2. Transverse magnetic in a waveguide

To test these boundary conditions in a waveguide, we simulated the transverse magnetic problem using the solution

$$E_z = \mu \frac{\partial \phi}{\partial t}, \qquad H_x = -\frac{\partial \phi}{\partial y}, \qquad H_y = \frac{\partial \phi}{\partial x}, \tag{62}$$

where ϕ is a solution of the scalar wave equation satisfying zero Dirichlet (PEC) boundary conditions at $y = 0$ and $y = 1$ produced by a point source centered at $(0, 0.1)$ with a time amplitude $\exp(-125(t + .475)^2)$. The DAB and PML boundaries were placed at $x = \pm 1$.

Again, we compare our results to a PML with parameters $\alpha_{max} = 0.25$ and $\kappa_{max} = 0.15$ in Fig. 3. We note that we have chosen to do our tests using a convolution PML [8] because it more effective at absorbing evanescent waves than
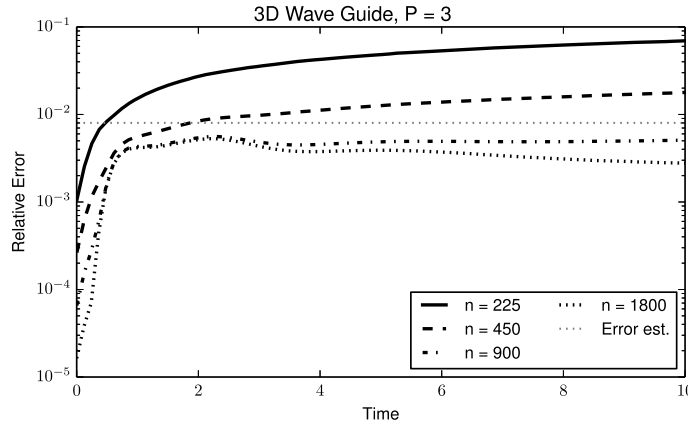
Fig. 4. Relative Error for the 3D wave guide problem using DAB boundaries with 3 CRBC recursions.
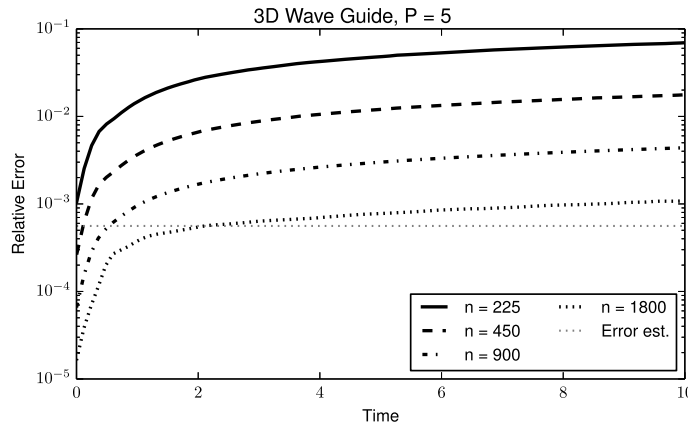
Fig. 5. Relative Error for the 3D wave guide problem using DAB boundaries with 5 CRBC recursions.

standard PMLs. We show the results for choosing $\sigma_{max} \approx 35000$, which corresponds to values recommended in [8] and $\sigma_{max} \approx 10000$ to illustrate the importance of parameter selection for PML accuracy. The refined grid uses $\sigma_{max} \approx 70000$. Here, we see that the DAB boundaries, which have automated parameter tuning, perform much better than the PML with the parameters tested. We believe that the difference in error between the PML and DAB is due to how well the boundaries handle evanescent waves; error estimates for the Bérenger PML on the continuous level, which can be deduced from the reflection analyses in [9,10], do indicate that to maintain accuracy over long times in waveguide geometry one must use a thick layer. Enhancements of the Bérenger PML to deal with evanescent modes have been proposed [11–13], but we do not know how their performance compares with the CPML used in our experiments.

4.3. 3D wave guide

For our tests in 3D, we use a solution to Maxwell's equations of the form

$$\mathbf{E} = -\mu \left(\nabla \times \frac{\partial \mathbf{W}}{\partial t} \right), \tag{63}$$

$$\mathbf{H} = \nabla \times (\nabla \times \mathbf{W}). \tag{64}$$

We choose $\mathbf{W}$ to be the point source solution to the vector wave equation $\mathbf{W} \equiv \frac{e^{-\gamma(t+\tau-r)^2}}{r}[1, 1, 1]^T$, where γ and τ are parameters and $r = \|\mathbf{x} - \mathbf{x}_{src}\|$. Using a solution generated from a point source located at $\mathbf{x}_{src} = [0.8, 0.8, 0.8]$ with $\tau = 0.39$ and $\gamma = 130$, we tested our implementation on the domain $[0, 1.6]^3$ with DAB boundaries at $x = 0$ and $x = 1.6$ and PEC boundaries elsewhere. The simulations were run with the DAB parameter $P = 3$ and $P = 5$ on a grid with n Yee cells in each spatial direction.

The results for various mesh spacings are displayed in Figs. 4 and 5. We also show the *a priori* error estimate computed by the optimization routine. We are able to reduce the error below the estimate for $P = 3$, which is approximately 1%, using a grid of 900^3. With further refinement using $P = 3$, the boundary error dominates and we see virtually no improvement
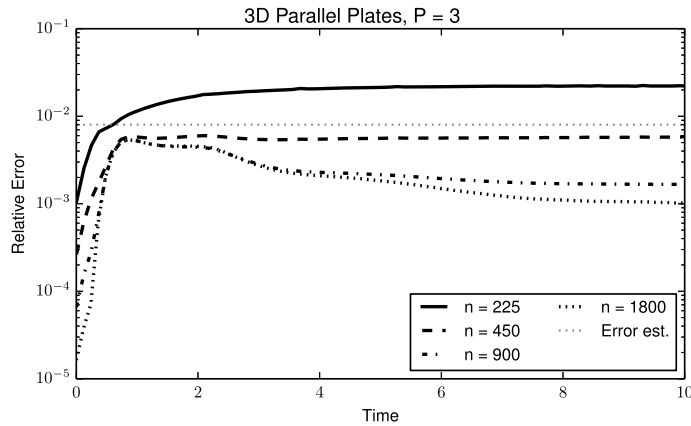
Fig. 6. Relative Error for the 3D parallel plate problem using DAB boundaries with 3 CRBC recursions.
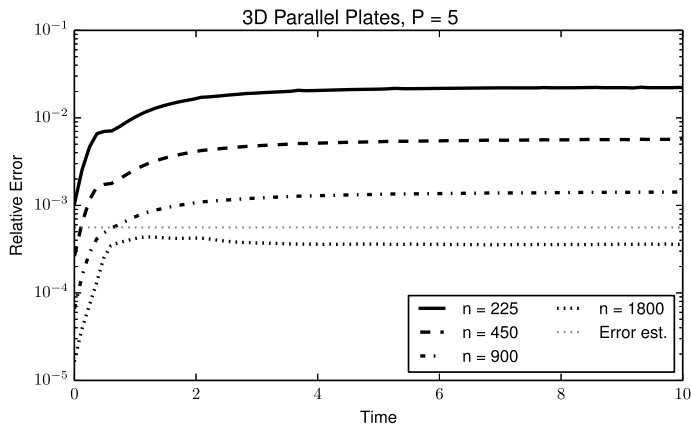

Fig. 7. Relative Error for the 3D parallel plate problem using DAB boundaries with 5 CRBC recursions.

in error. For $P = 5$ the grid would have to be refined again by a factor of approximately two in order to reduce the error below the estimate. Again we note that the *a priori* error estimates are achieved on sufficiently fine grids.

4.4. Parallel plates

Using the same source parameters as in Sec. 4.3, we set DAB boundaries at $x = 0$, $x = 1.6$, $y = 0$, and $y = 1.6$ and PEC boundaries elsewhere.

In Figs. 6 and 7 we see the behavior is similar to the wave guide problem in Figs. 4 and 5 but we observe slightly better errors in this case. We believe this is due to the fact that, on average, waves have a shorter residence time in the computational domain and thus experience less numerical dispersion. In this case, we are able to reduce the error below the estimate for $P = 5$.

4.5. Free space

Again, for the source parameters described Sec. 4.3, we use DAB boundaries on all of the boundary faces.

In Figs. 8 and 9 we see the performance appears to be much better. In terms of error, this is the easiest test case because the waves leave the computational domain quickly and impact the boundaries at near-normal incidence. It is worth noting that the stair stepping behavior of the error in Figs. 8 and 9 is caused by errors reflecting across the domain and each decrease of error corresponds to the predicted reflection coefficient of the boundary. The errors at long times are the same for both $P = 3$ and $P = 5$ because the erroneously reflected waves have had ample time to travel across the domain and be absorbed by the boundaries. We then see only the discretization error.

4.6. Comments on cost

Comparing the cost of the DAB layer to PML is not straightforward. Ideally, we would like to compare the accuracy of the DAB and PML boundaries of comparable costs. This is problematic because the performance of the PML is heavily dependent
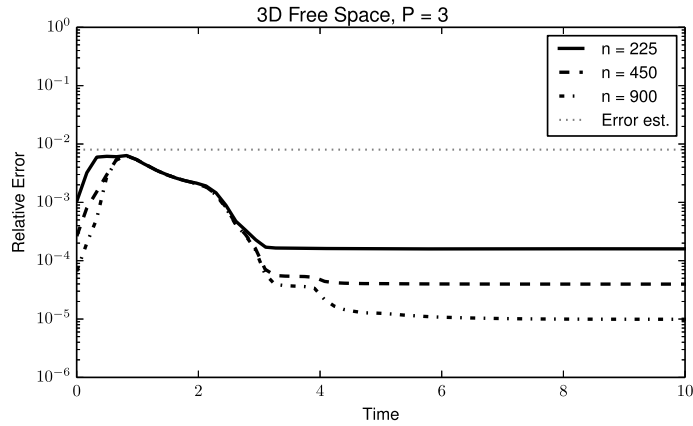
Fig. 8. Relative Error for the 3D free space problem using DAB boundaries with 3 CRBC recursions.
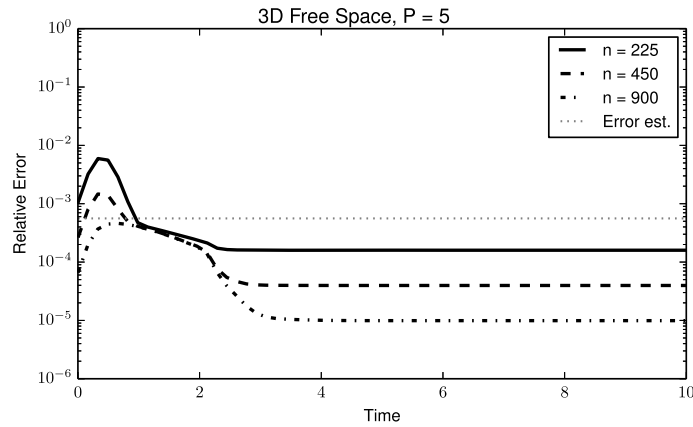

Fig. 9. Relative Error for the 3D free space problem using DAB boundaries with 5 CRBC recursions.

on the selection of parameters, which we again emphasize is an open problem (see e.g. [2]). Nonetheless, we can count the flops assuming that we have precomputed coefficients when possible.

In three dimensions, the PML implementation we have used [8] has the following costs per node in the tangential directions:

$$C_{PML}^{\pm}(w) = 36w, \qquad C_{PML}^{\times}(w) = 24w, \tag{65}$$

where $C_{PML}^{\pm}(w)$ is the number of addition/subtraction operations and $C_{PML}^{\times}(w)$ is the number of multiplications as a function of the thickness, w; that is the number of points in the normal direction in the layer. We note that other forms of the PML may have significantly different costs and there are potentially large setup costs associated with the selection of good PML parameters.

Similarly, the worst case cost of updating the DAB layer for all three **E** field components as a function of the number of recursions, P, is given by

$$C_{DAB}^{\pm}(P) = 60P + 39, \qquad C_{DAB}^{\times}(P) = 57P + 21. \tag{66}$$

We can see that the theoretical computational cost of a PML 10 cells thick is somewhat cheaper than using 5 recursions in the DAB in the worst case scenario. If there are no edges or corners present, then the DAB only needs to update the tangential **E** field components, which results in the reduced computational costs

$$C_{DAB}^{\pm}(P) = 40P + 26, \qquad C_{DAB}^{\times}(P) = 38P + 14. \tag{67}$$

In this case, the DAB with 5 recursions is theoretically cheaper than the PML with a width of 10.

We again emphasize that these statements are only meaningful if there is also a guarantee of similar effectiveness for both boundary types. In this regard, we believe the DAB boundaries may often be more efficient in practice because the DAB requires essentially no setup costs associated with finding good parameters. In contrast it may be necessary to run multiple simulations to identify reasonable PML parameters. Moreover in waveguide geometries we have been able to achieve significantly better accuracy than any PML we have tried.

5. Code

Code that is capable of reproducing most of the results presented here along with a library to provide the discretization of the DAB boundaries is available for download at http://www.rbcpack.org.

6. Conclusions and generalizations

We have demonstrated a convenient and automatic DAB implementation of CRBCs for electromagnetic waves in homogeneous, dielectric media, using modules from our open-source library. In our experiments for free space problems we have achieved accuracy/cost performance somewhat better than implementations of CPML suggested in the literature, while our results in waveguide geometries were significantly more accurate.

Generalizations of our algorithms to more complex models in the far field are theoretically possible, though we have not yet implemented them for the Maxwell system. In [14] we demonstrate the effectiveness of CRBCs in stratified media using parameters optimized for the maximum wave speed. We expect this approach will work well for layered dielectric media. Anisotropic media typically pose a greater challenge in terms of finding parameters which guarantee exponential convergence and we have not yet considered this problem for electromagnetic waves. This is clearly an important topic for future work.

Appendix A. Explicit DAB update formulas

The explicit update formulas for the DAB equations given in Sec. 2.3 are provided here for convenience. The wave equation updates (33)–(35) are of the form

$$v_{i,j,p}^{n+1} = 2v_{i,j,p}^n - v_{i,j,p}^{n-1} + c(\Delta t)^2 \left(\frac{v_{i-1,j,p}^n - 2v_{i,j,p}^n + v_{i+1,j,p}^n}{h_x^2} + \frac{v_{i,j-1,p}^n - 2v_{i,j,p}^n + v_{i,j+1,p}^n}{h_y^2} \right). \tag{A.1}$$

The recursions (37) and (18) can be solved for an explicit update in the "forward" direction on the interface side, for example recursions in the x-direction:

$$\left(\bar{a}_p + \frac{\Delta t}{h_x} + \frac{\Delta t}{2} \bar{\sigma}_p \right) v_{i,j,p+1}^{n+1} = \left(\bar{a}_p - \frac{\Delta t}{h_x} - \frac{\Delta t}{2} \bar{\sigma}_p \right) v_{i,j,p+1}^n$$
$$+ \left(\bar{a}_p + \frac{\Delta t}{h_x} - \frac{\Delta t}{2} \bar{\sigma}_p \right) v_{i+1,j,p+1}^n + \left(-a_p + \frac{\Delta t}{h_x} + \frac{\Delta t}{2} \sigma_p \right) v_{i+1,j,p}^n$$
$$+ \left(-a_p - \frac{\Delta t}{h_x} + \frac{\Delta t}{2} \sigma_p \right) v_{i,j,p}^n + \left(-\bar{a}_p + \frac{\Delta t}{h_x} - \frac{\Delta t}{2} \bar{\sigma}_p \right) v_{i+1,j,p+1}^{n+1}$$
$$+ \left(a_p + \frac{\Delta t}{h_x} + \frac{\Delta t}{2} \sigma_p \right) v_{i+1,j,p}^{n+1} + \left(a_p - \frac{\Delta t}{h_x} + \frac{\Delta t}{2} \sigma_p \right) v_{i,j,p}^{n+1}. \tag{A.2}$$

The recursions in the y-direction, (36) and (17), are essentially identical, but the differencing is done on the index j instead of i.

Similarly, the recursions (37) can be solved for an explicit update in the "backward" direction on the interface side, for example recursions in the x-direction:

$$\left(a_p + \frac{\Delta t}{h_x} + \frac{\Delta t}{2} \sigma_p \right) v_{i,j,p}^{n+1} = \left(a_p - \frac{\Delta t}{h_x} - \frac{\Delta t}{2} \sigma_p \right) v_{i,j,p}^n$$
$$+ \left(a_p + \frac{\Delta t}{h_x} - \frac{\Delta t}{2} \sigma_p \right) v_{i-1,j,p}^n + \left(-\bar{a}_p + \frac{\Delta t}{h_x} + \frac{\Delta t}{2} \bar{\sigma}_p \right) v_{i-1,j,p+1}^n$$
$$+ \left(-\bar{a}_p - \frac{\Delta t}{h_x} + \frac{\Delta t}{2} \bar{\sigma}_p \right) v_{i,j,p+1}^n + \left(-a_p + \frac{\Delta t}{h_x} - \frac{\Delta t}{2} \sigma_p \right) v_{i-1,j,p}^{n+1}$$
$$+ \left(\bar{a}_p + \frac{\Delta t}{h_x} + \frac{\Delta t}{2} \bar{\sigma}_p \right) v_{i-1,j,p+1}^{n+1} + \left(\bar{a}_p - \frac{\Delta t}{h_x} + \frac{\Delta t}{2} \bar{\sigma}_p \right) v_{i,j,p+1}^{n+1}. \tag{A.3}$$

Finally, the termination conditions (41) yield explicit updates of the form

$$\left(1 + \frac{c\Delta t}{h_x} \right) v_{i,j,P}^{n+1} = v_{i,j,k,Q}^n + v_{i-1,j,P}^n - v_{i-1,j,P}^{n+1}$$
$$+ \frac{c\Delta t}{h_x} \left(v_{i-1,j,P}^{n+1} - v_{i,j,P}^n + v_{i-1,j,P}^n \right) \tag{A.4}$$

for the x-direction.

Appendix B. Explicit procedure for the Yee scheme

We will consider the Yee scheme as described in Sec. 3 with a maximum of n_x, n_y, and n_z grid points in the x, y, and z directions respectively. In particular, there are $(n_x - 1, n_y, n_z)$ grid points for the E_x component and $(n_x, n_y - 1, n_z - 1)$ grid points for the H_x, for example, due to the staggered grid.

B.1. DAB face updates

For faces with DAB boundary conditions that are not adjacent to other DAB faces, we only require the DAB updates for the tangential **E** field components. For example, we will consider the left boundary face in the x-direction. In this case, the tangential components are E_y and E_z, so we introduce a three point layer of auxiliary variables that overlap the computational domain by two points for each of the components:

$$\left(\tilde{E}_y\right)^{1/2}_{i,j+1/2,k,p} = 0, \quad i = 0, 1, 2, \quad j = 1, ..., n_y - 1,$$
$$k = 1, ..., n_z, \quad p = 0, ..., P, \tag{B.1}$$

$$\left(\tilde{E}_z\right)^{1/2}_{i,j,k+1/2,p} = 0, \quad i = 0, 1, 2, \quad j = 1, ..., n_y,$$
$$k = 1, ..., n_z - 1, \quad p = 0, ..., P. \tag{B.2}$$

We next apply the DAB updates as described for scalar waves in Sec. 2.3. In particular, assuming we have evolved the interior values with the Yee scheme updates to time $t = (n + 1/2)\Delta t$ for the **E** fields, we first copy the last plane of points with updates into the auxiliary variables:

$$\left(\tilde{E}_y\right)^{n+1/2}_{2,j+1/2,k,0} = \left(E_y\right)^{n+1/2}_{2,j+1/2,k}, \tag{B.3}$$

$$\left(\tilde{E}_z\right)^{n+1/2}_{2,j,k+1/2,0} = \left(E_z\right)^{n+1/2}_{2,j,k+1/2}. \tag{B.4}$$

Next, we update the interior of the DAB layer using the second order, centered difference approximation to the wave equation:

$$\left(D_t^+ D_t^- - c^2 \left(D_x^+ D_x^- + D_y^+ D_y^- + D_z^+ D_z^-\right)\right)\left(\tilde{E}_y\right)^{n-1/2}_{1,j+1/2,k,p} = 0,$$
$$j = 2, ..., n_y - 2, \quad k = 2, ..., n_z - 1, \quad p = 0, ..., P, \tag{B.5}$$

$$\left(D_t^+ D_t^- - c^2 \left(D_x^+ D_x^- + D_y^+ D_y^- + D_z^+ D_z^-\right)\right)\left(\tilde{E}_z\right)^{n-1/2}_{1,j,k+1/2,p} = 0,$$
$$j = 2, ..., n_y - 1, \quad k = 2, ..., n_z - 2, \quad p = 0, ..., P. \tag{B.6}$$

We note that this gives the 3D equivalent of (A.1), which provides explicit updates for $\left(\tilde{E}_y\right)^{n+1/2}_{1,j+1/2,k,p}$ and $\left(\tilde{E}_z\right)^{n+1/2}_{1,j,k+1/2,p}$.

We can also handle the adjacent boundary conditions here. For illustration, we consider the adjacent boundaries to be perfect electric conductors (PEC). PEC boundaries can be enforced in the Yee scheme by setting homogeneous Dirichlet conditions on the tangential **E** field components to the boundary and homogeneous Neumann conditions on the normal **E** field component. Since the DAB updates have not been used on the boundaries, the tangential components should already be correctly set to 0. However, we need to deal with the normal components. We do this by substituting the discrete approximation to the homogeneous Neumann condition into the discrete wave equation updates to get

$$D_t^+ D_t^- \left(\tilde{E}_y\right)^{n-1/2}_{1,\frac{3}{2},k,p} - c^2 \left(\left[D_x^+ D_x^- + D_z^+ D_z^-\right]\left(\tilde{E}_y\right)^{n-1/2}_{1,\frac{3}{2},k,p}\right.$$
$$\left. + h_y^{-2}\left[-\left(\tilde{E}_y\right)^{n-1/2}_{1,\frac{3}{2},k,p} + \left(\tilde{E}_y\right)^{n-1/2}_{1,\frac{5}{2},k,p}\right]\right) = 0,$$
$$k = 2, ..., n_z - 1, \quad p = 0, ..., P, \tag{B.7}$$

$$D_t^+ D_t^- \left(\tilde{E}_y\right)^{n-1/2}_{1,n_y-1/2,k,p} - c^2 \left(\left[D_x^+ D_x^- + D_z^+ D_z^-\right]\left(\tilde{E}_y\right)^{n-1/2}_{1,n_y-1/2,k,p}\right.$$
$$\left. + h_y^{-2}\left[-\left(\tilde{E}_y\right)^{n-1/2}_{1,n_y-1/2,k,p} + \left(\tilde{E}_y\right)^{n-1/2}_{1,n_y-\frac{3}{2},k,p}\right]\right) = 0,$$
$$k = 2, ..., n_z - 1, \quad p = 0, ..., P, \tag{B.8}$$

$$D_t^+ D_t^- \left(\tilde{E}_z \right)_{1,j,\frac{3}{2},p}^{n-1/2} - c^2 \left(\left[D_x^+ D_x^- + D_y^+ D_y^- \right] \left(\tilde{E}_z \right)_{1,j,\frac{3}{2},p}^{n-1/2} \right.$$
$$\left. + h_z^{-2} \left[-\left(\tilde{E}_z \right)_{1,j,\frac{3}{2},p}^{n-1/2} + \left(\tilde{E}_z \right)_{1,j,\frac{5}{2},p}^{n-1/2} \right] \right) = 0, \tag{B.9}$$
$$j = 2, ..., n_y - 1, \quad p = 0, ..., P,$$

$$D_t^+ D_t^- \left(\tilde{E}_z \right)_{1,j,n_z-1/2,p}^{n-1/2} - c^2 \left(\left[D_x^+ D_x^- + D_y^+ D_y^- \right] \left(\tilde{E}_z \right)_{1,j,n_z-1/2,p}^{n-1/2} \right.$$
$$\left. + h_z^{-2} \left[-\left(\tilde{E}_z \right)_{1,j,n_z-1/2,p}^{n-1/2} + \left(\tilde{E}_z \right)_{1,j,n_z-\frac{3}{2},p}^{n-1/2} \right] \right) = 0, \tag{B.10}$$
$$j = 2, ..., n_y - 1, \quad p = 0, ..., P.$$

Next, we can apply the Sommerfeld termination conditions:

$$\left(D_t^+ A_x^+ - c D_x^+ A_t^+ \right) \left(\tilde{E}_y \right)_{0,j+1/2,k,P}^{n-1/2} = 0, \tag{B.11}$$
$$j = 1, ..., n_y - 1, \quad k = 1, ..., n_z,$$

$$\left(D_t^+ A_x^+ - c D_x^+ A_t^+ \right) \left(\tilde{E}_z \right)_{0,j,k+1/2,P}^{n-1/2} = 0, \tag{B.12}$$
$$j = 1, ..., n_y, \quad k = 1, ..., n_z - 1.$$

Note that there is a sign change from the explicit update formula (A.4) because the outward normal from the face we are considering is $x = -1$ whereas (A.4) are given for the outward normal $x = 1$.

Now we can apply the CRBC recursions (again, noting the sign change due to the outward normal direction):

$$\left(\bar{a}_j D_t^+ A_x^+ + D_x^+ A_t^+ + \bar{\sigma}_j A_t^+ A_x^+ \right) \left(\tilde{E}_y \right)_{i,j+1/2,k,p+1}^{n-1/2} =$$
$$\left(a_j D_t^+ A_x^+ - D_x^+ A_t^+ + \sigma_j A_t^+ A_x^+ \right) \left(\tilde{E}_y \right)_{i,j+1/2,k,p}^{n-1/2}, \tag{B.13}$$
$$i = 0, 1, \quad j = 1, ..., n_y - 1, \quad k = 1, ..., n_z,$$

$$\left(\bar{a}_j D_t^+ A_x^+ + D_x^+ A_t^+ + \bar{\sigma}_j A_t^+ A_x^+ \right) \left(\tilde{E}_z \right)_{i,j,k+1/2,p+1}^{n-1/2} =$$
$$\left(a_j D_t^+ A_x^+ - D_x^+ A_t^+ + \sigma_j A_t^+ A_x^+ \right) \left(\tilde{E}_z \right)_{i,j,k+1/2,p}^{n-1/2}, \tag{B.14}$$
$$i = 0, 1, \quad j = 1, ..., n_y, \quad k = 1, ..., n_z - 1.$$

Finally, we can provide the updated values to the interior Yee scheme updater:

$$\left(E_y \right)_{1,j+1/2,k}^{n+1/2} = \left(\tilde{E}_y \right)_{1,j+1/2,k,0}^{n+1/2}, \tag{B.15}$$

$$\left(E_z \right)_{1,j,k+1/2}^{n+1/2} = \left(\tilde{E}_z \right)_{1,j,k+1/2,0}^{n+1/2}. \tag{B.16}$$

B.2. DAB edges

If there are two or more adjacent DAB layers, we cannot update points at the intersecting edge as described. In particular, we cannot apply updates analogous to (B.7)–(B.10). Additionally, to update an edge we require auxiliary data from the normal components on the intersecting faces. To get this data, we simply perform DAB face updates described in Appendix B.1 on the normal component; however, we omit the last step of copying the values back into the interior because the Yee scheme should have correctly updated the points.

To illustrate the edge conditions, we'll consider the intersection of two faces: one with a outward normal $x = -1$ and the other with the outward normal $y = 1$. We will assume that we have updated all of the auxiliary variables that we can on each of the faces, so we have

$$\left(\tilde{E}_x \right)_{i+1/2,j,k,p}^{n+1/2}, \quad i = 0, 1, 2 \quad j = 1, ..., n_y - 1, \quad k = 1, ..., n_z, \tag{B.17}$$

$$\left(\tilde{E}_y \right)_{j,j+1/2,k,p}^{n+1/2}, \quad i = 0, 1, 2 \quad j = 1, ..., n_y - 2, \quad k = 1, ..., n_z, \tag{B.18}$$

$$\left(\tilde{E}_z\right)^{n+1/2}_{k,j,k+1/2,p}, \quad i=0,1,2 \quad j=1,...,n_y-1,$$
$$k=1,...,n_z-1, \tag{B.19}$$

$$\left(\hat{E}_x\right)^{n+1/2}_{i+1/2,j,k,q}, \quad i=2,...,n_x-1 \quad j=n_y-1,n_y,n_y+1,$$
$$k=1,...,n_z, \tag{B.20}$$

$$\left(\hat{E}_y\right)^{n+1/2}_{j,j+1/2,k,q}, \quad i=2,...,n_x \quad j=n_y-2,n_y-1,n_y,$$
$$k=1,...,n_z, \tag{B.21}$$

$$\left(\hat{E}_z\right)^{n+1/2}_{k,j,k+1/2,q}, \quad i=2,...,n_x \quad j=n_y-1,n_y,n_y+1,$$
$$k=1,...,n_z-1, \tag{B.22}$$

where we use $\tilde{E}$ to denote the auxiliary variables on the face with normal $x=-1$ and $\hat{E}$ to denote the auxiliary variables on the face with normal $y=1$. For the E_x components, we need to calculate updates at the spatial location $(1,n_y,k)$ for $k=1,...,n_z$. Similarly, we need updates at $(1,n_y-1,k)$ and $(1,n_y,k)$ for E_y and E_z, respectively. In each case, the process is the same, so we only consider the case for the E_z component. We begin by introducing a doubly indexed set of auxiliary variables that overlaps the auxiliary variables $\tilde{E}_z$ and $\hat{E}_z$

$$\left(\bar{E}_z\right)^{1/2}_{i,j,k+1/2,p,q}=0, \quad i=\{0,1,2\}, \quad j=n_y-1,n_y,n_y+1$$
$$k=1,...,n_z-1, \quad p=0,...,P, \quad q=0,...,P, \tag{B.23}$$

where we assume that there are the same number $(P+1)$ of auxiliary variables on each of the faces. We will additionally assume that the auxiliary equations on each of the faces uses the same CRBC parameters although in general this need not be the case. We use the convention that the p index corresponds to recursions in the x direction and the q index corresponds to recursions in the y direction.

We input the data from the faces into the edge auxiliary variables:

$$\left(\bar{E}_z\right)^{n+1/2}_{1,n_y-1,k+1/2,p,0}=\left(\tilde{E}_z\right)^{n+1/2}_{1,n_y-1,k+1/2,p} \tag{B.24}$$

$$\left(\bar{E}_z\right)^{n+1/2}_{2,n_y,k+1/2,0,q}=\left(\hat{E}_z\right)^{n+1/2}_{2,n_y,k+1/2,q} \tag{B.25}$$

Next we update the interior points for all of the auxiliary variables using the wave equation

$$D_t^+D_t^-\left(\bar{E}_z\right)^{n-1/2}_{1,n_y,k+1/2,p,q}$$
$$-c^2\left(D_x^+D_x^-+D_y^+D_y^-+D_z^+D_z^-\right)\left(\bar{E}_z\right)^{n-1/2}_{1,n_y,k+1/2,p,q}=0, \tag{B.26}$$
$$k=2,...,n_z-2, \quad p=0,...,P, \quad q=0,...,P.$$

We additionally apply any adjacent boundary conditions here as described in Appendix B.1 for the face updates. Then, we can apply the Sommerfeld termination conditions:

$$\left(D_t^+A_x^+-cD_x^+A_t^+\right)\left(\bar{E}_z\right)^{n-1/2}_{0,n_y,k+1/2,P,q}=0, \tag{B.27}$$
$$k=1,...,n_z-1, \quad q=0,...,P.$$

$$\left(D_t^+A_y^++cD_y^+A_t^+\right)\left(\bar{E}_z\right)^{n-1/2}_{1,n_y,k+1/2,p,P}=0, \tag{B.28}$$
$$k=1,...,n_z-1, \quad p=0,...,P.$$

Now we can apply the CRBC recursions (again, noting the sign change due to the outward normal direction):

$$\left(\bar{a}_jD_t^+A_x^++D_x^+A_t^++\bar{\sigma}_jA_t^+A_x^+\right)\left(\bar{E}_z\right)^{n-1/2}_{i,n_y,k+1/2,p+1,q}=$$
$$\left(a_jD_t^+A_x^+-D_x^+A_t^++\sigma_jA_t^+A_x^+\right)\left(\bar{E}_z\right)^{n-1/2}_{i,n_y,k+1/2,p,q}, \tag{B.29}$$
$$i=0,1, \quad k=1,...,n_z-1.$$

$$\left(\bar{a}_jD_t^+A_j^+-D_j^+A_t^++\bar{\sigma}_jA_t^+A_j^+\right)\left(\bar{E}_z\right)^{n-1/2}_{1,j,k+1/2,p,q+1}=$$
$$\left(a_jD_t^+A_y^++D_y^+A_t^++\sigma_jA_t^+A_y^+\right)\left(\bar{E}_z\right)^{n-1/2}_{1,n_y,k+1/2,p,q}, \tag{B.30}$$
$$j=n_y-1,n_y, \quad k=1,...,n_z-1.$$

Finally, we can provide the updated values to the interior Yee scheme updater and the auxiliary variables on the faces:

$$(E_z)_{1,n_y,k+1/2}^{n+1/2} = (\bar{E}_z)_{1,n_y,k+1/2,0,0}^{n+1/2}, \tag{B.31}$$

$$\left(\tilde{E}_z\right)_{1,n_y,k+1/2,p}^{n+1/2} = (\bar{E}_z)_{1,n_y,k+1/2,p,0}^{n+1/2}, \tag{B.32}$$

$$\left(\hat{E}_z\right)_{1,n_y,k+1/2,q}^{n+1/2} = (\bar{E}_z)_{1,n_y,k+1/2,0,q}^{n+1/2}. \tag{B.33}$$

We note that corners are handled analogously by introducing a triply index set of auxiliary variables.

References

[1] J.-P. Berenger, A perfectly matched layer for the absorption of electromagnetic waves, J. Comput. Phys. 114 (2) (1994) 185–200, http://dx.doi.org/10.1006/jcph.1994.1159, http://www.sciencedirect.com/science/article/pii/S0021999184711594.

[2] A. Modave, E. Delhez, C. Geuzaine, Optimizing perfectly matched layers in discrete contexts, Int. J. Numer. Methods Eng. 99 (6) (2014) 410–437, http://dx.doi.org/10.1002/nme.4690.

[3] T. Hagstrom, T. Warburton, Complete radiation boundary conditions: minimizing the long time error growth of local methods, SIAM J. Numer. Anal. 47 (5) (2009) 3678–3704, http://dx.doi.org/10.1137/090745477, http://epubs.siam.org/doi/pdf/10.1137/0907454.

[4] K. Stein, Complete radiation boundary conditions: corner and edge closure conditions, Ph.D. thesis, Southern Methodist University, 2012.

[5] T. Hagstrom, D. Givoli, D. Rabinovich, J. Bielak, The double absorbing boundary method, J. Comput. Phys. 259 (2014) 220–241, http://dx.doi.org/10.1016/j.jcp.2013.11.025, http://www.sciencedirect.com/science/article/pii/S0021999113007870.

[6] K. Yee, Numerical solution of initial boundary value problems involving Maxwell's equations in isotropic media, IEEE Trans. Antennas Propag. 14 (3) (1966) 302–307, http://dx.doi.org/10.1109/TAP.1966.1138693.

[7] X.R. Chen, D. Appelö, T. Hagstrom, A hybrid Hermite-discontinuous Galerkin method for hyperbolic systems with application to Maxwell's equations, J. Comput. Phys. 257 (2014) 501–520, http://dx.doi.org/10.1016/j.jcp.2013.09.046, http://www.sciencedirect.com/science/article/pii/S0021999113006608.

[8] J.A. Roden, S.D. Gedney, Convolution PML (CPML): an efficient FDTD implementation of the CFSPML for arbitrary media, Microw. Opt. Technol. Lett. 27 (5) (2000) 334–339, http://dx.doi.org/10.1002/1098-2760(20001205)27:5<334::AID-MOP14>3.0.CO;2-A.

[9] J. Diaz, P. Joly, A time domain analysis of {PML} models in acoustics, Comput. Methods Appl. Mech. Eng. 195 (2932) (2006) 3820–3853, http://dx.doi.org/10.1016/j.cma.2005.02.031, absorbing boundary conditions, http://www.sciencedirect.com/science/article/pii/S0045782505002604.

[10] A.T. de Hoop, P.M. van den Berg, R.F. Remis, Absorbing boundary conditions and perfectly matched layers – an analytic time-domain performance analysis, IEEE Trans. Magn. 38 (2) (2002) 657–660, http://dx.doi.org/10.1109/20.996171.

[11] Y.C. Lau, M.S. Leong, P.S. Kooi, Extension of Berenger's PML boundary condition in matching lossy medium and evanescent waves, Electron. Lett. 32 (11) (1996) 974–976, http://dx.doi.org/10.1049/el:19960627.

[12] J. Fang, Z. Wu, Generalized perfectly matched layer for the absorption of propagating and evanescent waves in lossless and lossy media, IEEE Trans. Microw. Theory Tech. 44 (12) (1996) 2216–2222, http://dx.doi.org/10.1109/22.556449.

[13] J.P. Berenger, An effective PML for the absorption of evanescent waves in waveguides, IEEE Microw. Guided Wave Lett. 8 (5) (1998) 188–190, http://dx.doi.org/10.1109/75.668706.

[14] T. Hagstrom, High-order radiation boundary conditions for stratified media and curvilinear coordinates, J. Comput. Acoust. 20 (02) (2012) 1240002, http://dx.doi.org/10.1142/S0218396X12400024, http://www.worldscientific.com/doi/pdf/10.1142/S0218396X12400024.